

PAPER • OPEN ACCESS

Modelling large-sized mesh reflector with extended aperture

To cite this article: S V Belov *et al* 2019 *J. Phys.: Conf. Ser.* **1145** 012006

View the [article online](#) for updates and enhancements.



IOP | ebooks™

Bringing together innovative digital publishing with leading authors from the global scientific community.

Start exploring the collection—download the first chapter of every title for free.

Modelling large-sized mesh reflector with extended aperture

S V Belov¹, A V Belkov, A P Zhukov, S V Ponomarev, M S Pavlov

National Research Tomsk State University, Tomsk, 36 Lenin Ave., 634050, Russia

¹E-mail: belovsv@niipmm.tsu.ru

Abstract. Offset large-sized deployable mesh reflector with symmetric frontal and rear nets is described in the paper. This reflector involves extended aperture area and reduced framework elements by applying beam elements in the peripheral areas of reflecting surface. Strain-stress analysis is conducted to calculate reflecting surface shape of required accuracy.

1. Introduction

Designing updated large-sized deployable space reflectors is one of the current issues in both military and industrial sectors. The practical relevance of such reflectors has been described in [1 – 3]. In the publications [4 – 6], different reflector types have been discussed, involving their stiffness estimation via mode shapes and relevant natural frequencies, as well as the analysis of various approaches in solving nonlinear problems for cable membrane structures, including initial estimate determination.

Antenna gain directly depends on the reflector aperture size. The more the reflector aperture is, the more its structure mass and dimension size is (due to extending framework spoke elements), which, in its turn, could be an unfavorable condition in transporting the reflector on-orbit. The research target is to design a large-sized deployable reflector with the following characteristics – less mass, increased aperture size and precise reflector surface.

2. Problem statement

Stress-strain state simulation problem of cable beam shell structures is based on nonlinear elasticity theory which includes thermal strain.

Deformation-displacement relation is considered as:

$$e_{ij} = (1/2)(u_{i,j} + u_{j,i} + u_{k,i}u_{k,j}), \quad (1)$$

where, u_i – components of the displacement vector.

To simulate the mechanical behavior in stress state, simplified stress-strain relations are applied. Tensor components of Kirchhoff stress and tensor components of strain are:

$$\sigma_{ij} = a_{ijkl}(e_{kl} - e_{kl}^{Temp}), \quad (2)$$

where, $a_{ijkl} = a_{ijkl}(X, T)$ – elasticity tensor components related to different structure elements and their temperatures; $e_{kl}^{Temp} = \mathcal{G} \delta_{kl} \Delta T$ – strain temperature tensor components; \mathcal{G} – linear thermal expansion coefficient; δ_{kl} – Kronecker symbol; $\Delta T = T - T_0$ – temperature difference; T_0 – initial temperature; T – final temperature. The next relation is the equilibrium equation:

$$[\sigma_{ij} \cdot (\delta_{ki} + u_{k,i})]_{,j} + P_i = 0, \quad (3)$$



where, P_i – mass force components.

Displacement boundary conditions are assigned to S_u structure surface, where $\mathbf{u}=0$ is the attachment location to the spacecraft. In the above-mentioned problem statement, the initial state is the zero stress of the elements in the reflector structure. Due to prescribed boundary conditions pretensioned structure is in the equilibrium state, providing a rather precise designed reflector surface shape.

Analytically, such problem tasks are difficult to solve. It is more preferable to apply the variational approach so as to receive numerical solutions. Detailed variational approach is described in [7].

Root mean square (RMS) error of reflecting surface δ_{rms} is expressed as paraboloid axis error Δz [8]:

$$\delta_{rms,z} = \left(\frac{1}{S_a} \iint_{S_a} (\Delta z)^2 dS \right)^{1/2}, \quad (4)$$

where, S_a – reflecting surface area.

This relation is a good approximation for any surface deflection in reference to the best fit paraboloid. In this case, it is preferable to apply the above-mentioned formula, not only for radiometric surface deflection approximation but also for imperfect surface gain loss [9].

In Cartesian coordinates (X, Y, Z) RMS error of structure nodes with coordinates x_i, y_i, z_i ($i=1, \dots, N$) is estimated by the integral formula:

$$RMS_z = \left(\frac{1}{N} \sum_{i=1}^N \Delta z_i^2 \right)^{1/2}, \quad (5)$$

where, $\Delta z_i = z_i - z_i^{ideal}$ – i -node deflection from paraboloid; z_i^{ideal} – theoretical value Z of i -node coordinate on paraboloid; N – number of points. It is presupposed that node distribution on reflecting surface influences the RMS error proportionally.

However, the systematic error is also involved in the RMS error:

$$\overline{\Delta z} = \frac{1}{N} \sum_{i=1}^N \Delta z_i. \quad (6)$$

This could easily exclude reflector displacement on Z axis. It is more suitable to use RMS error without the systematic error being calculated as:

$$RMS_z = \left(\frac{1}{N} \sum_{i=1}^N (\Delta z_i - \overline{\Delta z})^2 \right)^{1/2}. \quad (7)$$

3. Reflector structure elements

Applying beam elements within reflector peripheral sectors results in the increased aperture area which insignificantly changes the mass structure itself (figure 1).

The reflector size of not more than 36 m is illustrated in Figure 2. If beam elements are excluded, this would result in the increase of the framework structure elements to 5 m. In this case, this structure would be 45 m or more in size.

If the number of framework spokes are decreased (in our case to 6), the reflecting surface sector area would increase. In this case, the beam elements retain the effective reflecting surface area despite the decreasing number of spokes (figure 1, figure 2).

Figure 2–5 illustrate finite element model (FEM) offset mesh reflector with 6-spoke framework (35 m in diameter). Frontal and rear nets are symmetric.

FEM includes shell elements without bending stiffness (reflecting surface), one-dimensional cord elements (rear and frontal nets, tension ties, framework cords), shell elements with bending stiffness

(spoke elements), one-dimensional beam elements, hub designed as honeycomb structure between 2 carbon composite layers.

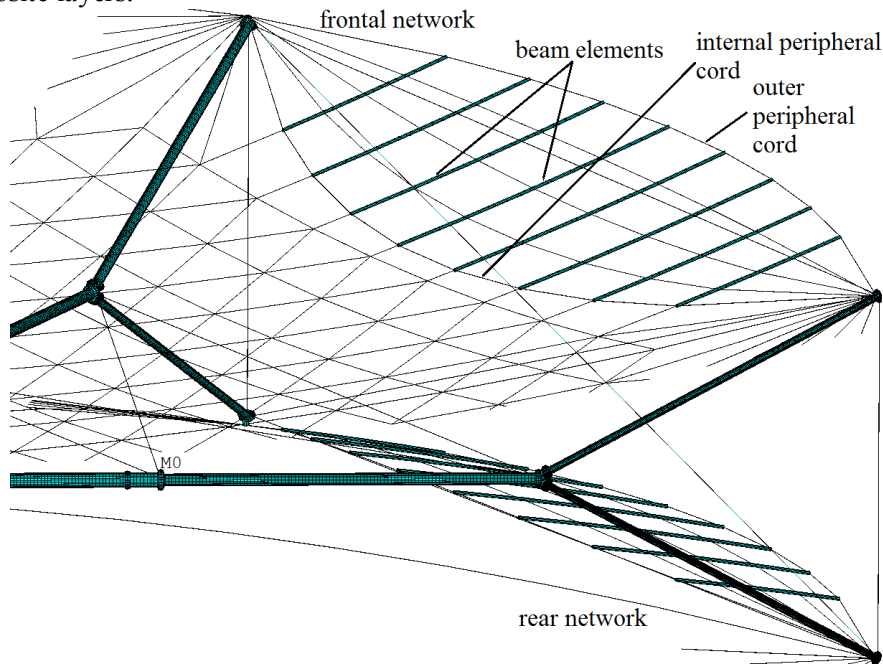


Figure 1. Reflector peripheral sector with beam elements.

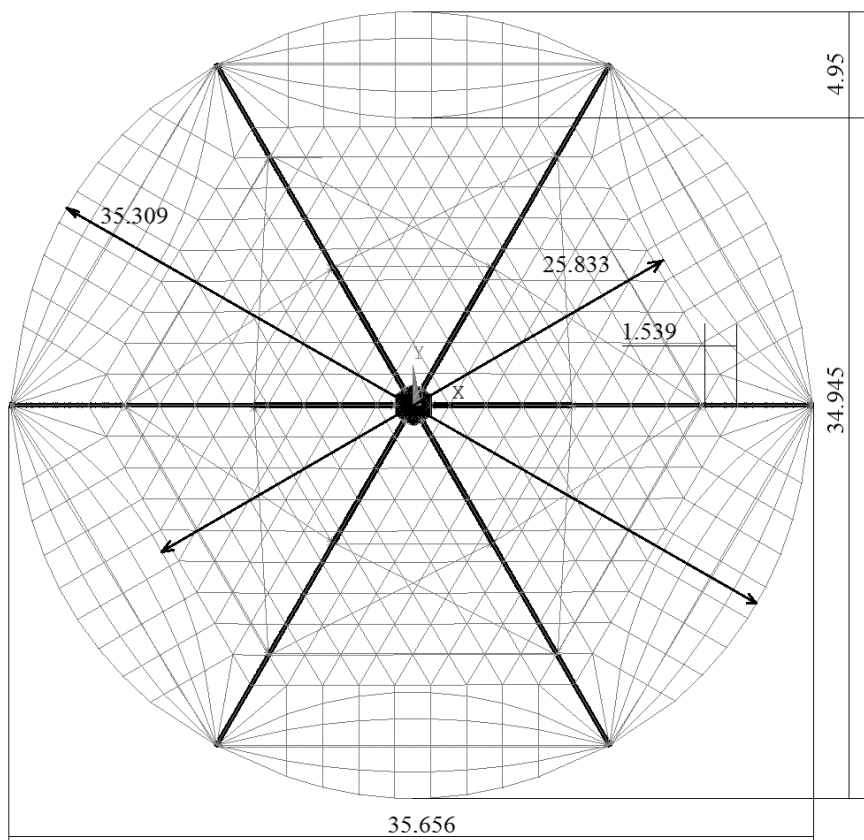


Figure 2. Geometrical reflector sizes, m.

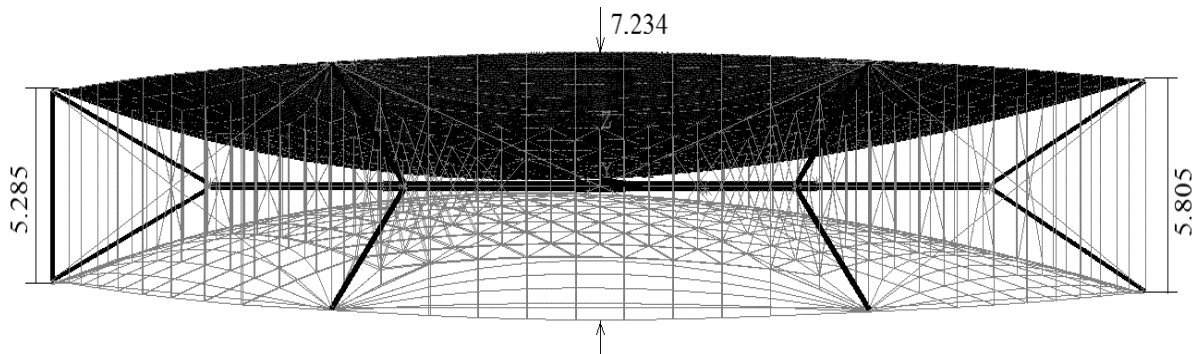


Figure 3. Geometrical reflector sizes, m.

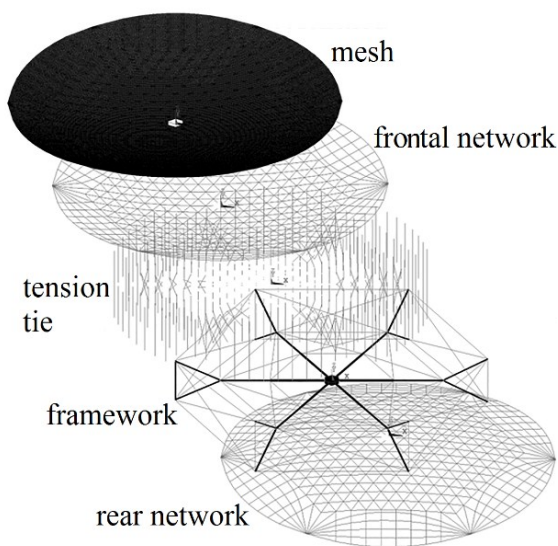


Figure 4. Component parts of FEM.

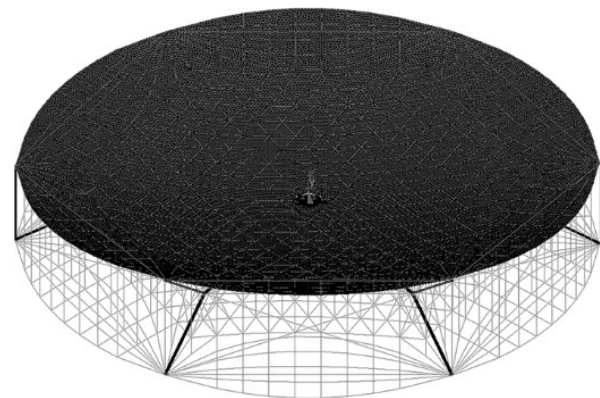


Figure 5. FEM of reflector.

Figure 6 illustrates spoke components and tension ties arrangement. Tension ties are fixed directly to root components, while other tension ties – indirectly from intermediate and A and B components.

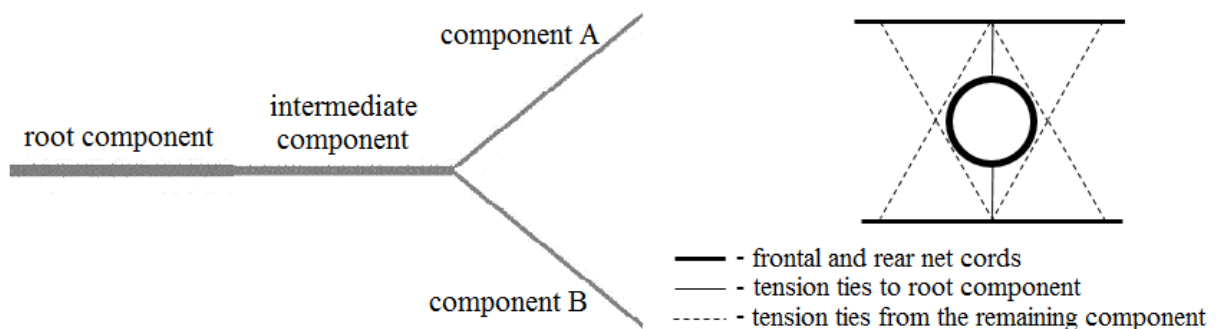


Figure 6. Spoke components and tension ties arrangement.

FEM elements characteristics:

- root components with circular tube section diameter of 0.218 m, wall thickness – 7×10^{-4} m, length – 6.158 m, elasticity modulus – 1.51×10^{11} Pa;
- intermediate component with circular tube section diameter of 0.179 m, length – 6.158 m, wall

- thickness – 7×10^{-4} m, elasticity modulus – 1.51×10^{11} Pa;
- component A and B with semi-circular section, wall thickness – 7×10^{-4} m, length – 5.639 m, elasticity modulus – 1.51×10^{11} Pa;
 - mesh, thickness – 1×10^{-4} m with initial tension of 2 N/m, elasticity modulus – 1.3×10^6 Pa;
 - hub diameter – 1.817 m, height – 0.28 m, honeycomb structure (carbon composite framework with elasticity modulus – 7.5×10^{10} Pa, honeycomb filler – aluminium with elasticity modulus $E_x=6.95 \times 10^5$ Pa, $E_y=6.95 \times 10^5$ Pa, $E_z=1.36 \times 10^9$ Pa; shear modulus $G_{xy}=1.3 \times 10^5$ Pa, $G_{yz}=1.9 \times 10^8$ Pa, $G_{xz}=1.27 \times 10^8$ Pa);
 - peripheral beam elements with circular tubesection diameter of 5×10^{-3} m, wall thickness – 7×10^{-4} m, elasticity modulus – 1.51×10^{11} Pa.

Table 1. Structure mass distribution.

Structure elements	Mass (kg)
Root component	29
Intermediate component	24
Components A and B	35
peripheral beam elements (frontal net)	6.65
peripheral beam elements (rear net)	6.65
Rigid brace	3.3
Hub	31
Framework cords	4.3
Frontal net	6.6
Rear net	6.6
Tension ties	0.17
Mesh	20
Deployment mechanism	72.6
Total mass	246

4. Results and discussion

According to calculation results, all considered stress-strain state parameters are within the range of satisfactory values. They are illustrated in figures 7-12.

Reflector surface is adjusted by 480 tension ties and 5 cords between components A and B as illustrated in figure 6. Figure 7 illustrates node displacement distributions of reflection surface from parabolic surface. RMS error of all adjusting nodes equals 4.8 mm and this shows a high accuracy of the reflector surface.

Stress intensity in framework elements (spokes) is depicted in figure 8, while node displacement of its elements in figure 9. As these values are insignificant, the reflector framework structure is well – balanced. Stress intensity in mesh is illustrated in figure 10, while tension distribution in sectors of frontal and rear net cords in figures 11, 12. Tension distribution in internal and outer peripheral cords (where peripheral beam elements are located) is illustrated in figures 13, 14. These results show that reflector cords are not slacked, i.e. non-zero tension values. This positively affects the reflector surface accuracy, relatively uniform element stress distribution values in the mesh, as well as the solution iterative process.

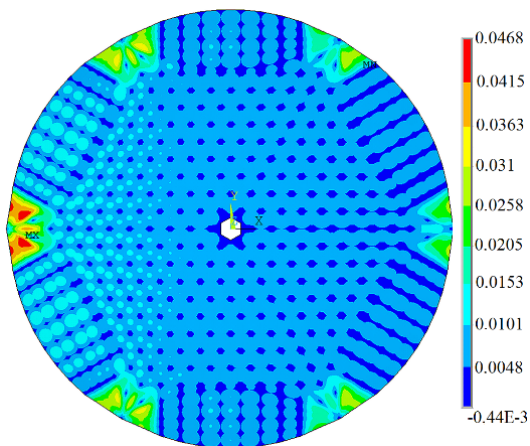


Figure 7. Node displacement distribution of reflection surface from parabolic surface, m. RMS=4.8 mm.

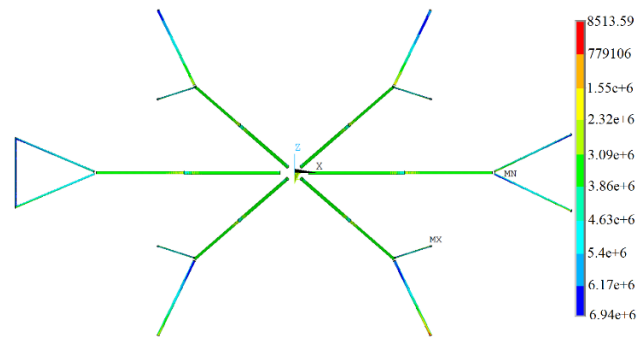


Figure 8. Stress intensity in framework elements (spokes), Pa.

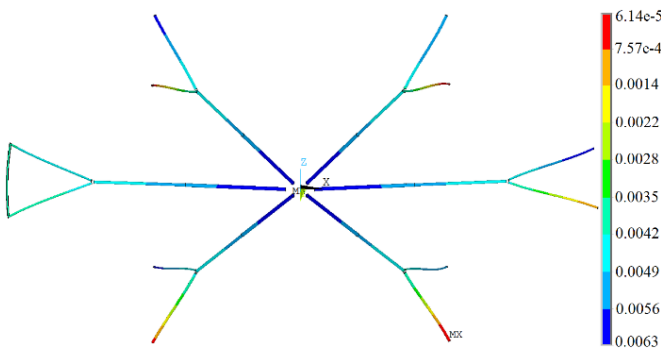


Figure 9. Node displacement of framework elements, m (visually zoomed up to 320)

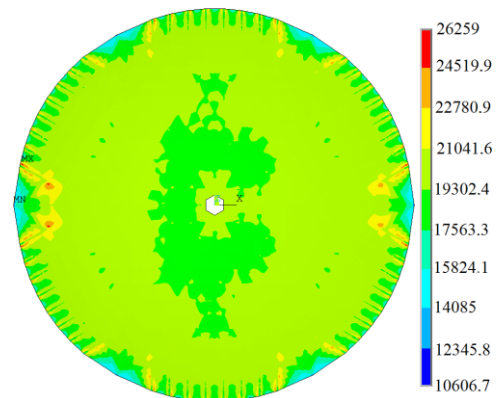


Figure 10. Stress intensity in mesh, Pa.

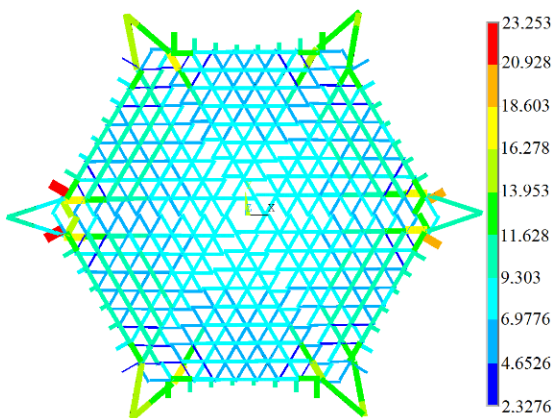


Figure 11. Tension distribution in sectors of frontal net cords, N.

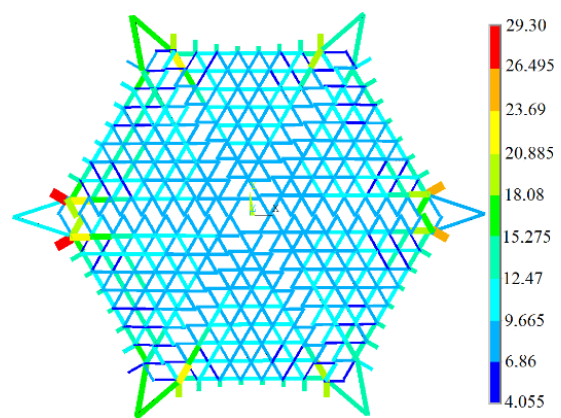


Figure 12. Tension distribution in sectors of rear net cords, N.

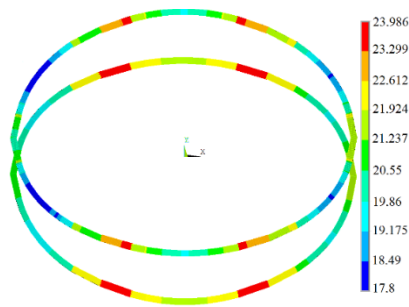


Figure 13. Tension distribution in outer peripheral cords, N.

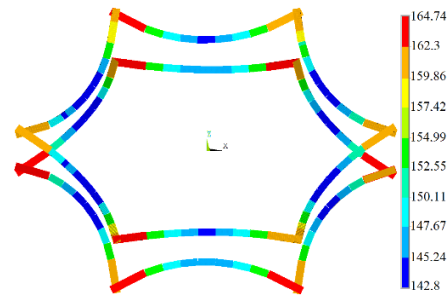


Figure 14. Tension distribution in internal peripheral cords, N.

5. Conclusion

Applying peripheral beam elements in frontal and rear network sectors, results in the increased aperture area, in significantly changing the mass structure (not more than 14 kg). These beam elements improve the reflecting surface accuracy within peripheral sector component, which, in its turn, leads to surface adjustment with RMS error not more than 5 mm.

To decrease RMS error, its necessary to add at least 2 beam elements in each sector. As there was no cord tension adjustment in frontal and rear nets, therefore, the tension distribution ranged from 2 N to 23 N. Cord tension adjustment within the sectors, ranging from 7.5 N to 12.5 N, allows increasing the reflector surface accuracy. In this case, there could be more outer and internal peripheral cord tension. To decrease structure mass and reduce complicated rear net topology, it's possible to exclude peripheral beam elements. However, this could negatively affect the reflecting surface accuracy within peripheral sector areas.

Acknowledgments

This work has been financially supported by Ministry of Education and Science of the Russian Federation. Unique identifier RFMEFI57517X0144. Agreement No 14.575.21.0144.

References

- [1] Chu Z, Deng Z, Qi X and Li B 2014 Modeling and analysis a large deployable antenna structure, *Acta Astronaut.* **95** 51
- [2] Tang Y, Li T, Wang Z and Deng H 2014 Surface accuracy analysis of large deployable antennas *Acta Astronaut.* **104** 125
- [3] Scialino L, Ihle A, Migliorelli M, Gatti N, Datashvili L, van 't Klooster K and Santiago Prowald J 2013 Large deployable reflectors for telecom and earth observation applications *CAES Space J.* **5** 125
- [4] Belkov A, Belov S, Pavlov M, Ponomarev V and Zhukov 2016 A Stiffness estimation for large-sized umbrella space reflector *MATEC Web of Conf.* **48** 02001 1-6
- [5] Belov S, Pavlov M, Ponomarev V, Ponomarev S and Zhukov A 2016 Calculation method for cable-beam shell structures. *XIII Int. Conf. on Prospects of Fundamental Sciences Development, PFSD 2016 (Tomsk, Russia)* **1772** 1-8
- [6] Ponomarev S, Zhukov A, Belkov A, Ponomarev V, Belov S, Pavlov M 2015 Stress-strain state simulation of large-sized cable-stayed shell structures. *IOP Conf. Series: Materials Science and Engineering* Vol. 71, 012070 1-7 doi:10.1088/1757-899X/71/1/012070
- [7] Washizu K *Variational Methods in Elasticity and Plasticity* 1982 (Oxford-New York: Pergamon Press) 424 p.
- [8] Greschik G, Palisoc A, Cassapakis C, Veal G, Mikulas M 2001 Sensitivity study of precision pressurized membrane reflector deformations *AIAA J.* **39** 2 308
- [9] Pontoppidan K 1984 Electrical consequences of mechanical antenna characteristics *Workshop on Mechanical Technology for Antennas, ESA/ESTEC (Noordwijk)* pp 41-47